from Experimental Compressibility Data," *Physica*, **33**, 481 (1967).
Hall, K. R., and F. B. Canfield, "Isotherms for the He-N_2 System at −190°C, −170°C and −160°C up to 700 atm," *Physica*, **47**, 219 (1970).
Hall, K. R., and P. T. Eubank, "Burnett-Isochoric Coupled Data with Application to Adsorbing Gases," *Physica*, **61**, 346 (1972).
Hall, K. R., and P. T. Eubank, "Experimental Technique for Direct Measurement of Interaction Second Virial Coefficients," *J. Chem. Phys.*, **59**, 709 (1973).
Hall, K. R., and P. T. Eubank, "Mixture Compositions and Excess Volumes from the Burnett Apparatus," *AIChE J.*, **20**, 815 (1974).
Hall, K. R., and W. Righter, "Optimal Truncation of the Virial Equation," *AIChE J.*, **21**, 406 (1975).
Harper, Jr., R. C., and J. G. Miller, "Compressibility of Gases II. Mixtures of Carbon Dioxide and Helium at 30°C," *J. Chem. Phys.*, **27**, No. 1, 36 (1957).
Hirschfelder, J. O., C. F. Curtiss, and R. B. Bird, "Molecular Theory of Gases and Liquids," 170, John Wiley and Sons, Inc., New York (1954).
Holste, J. C., P. T. Eubank, and K. R. Hall, "Optimum Use of a Differential Pressure Transducer for High-Precision Measurements," *Ind. Eng. Chem., Fund.*, **16**, 378 (1977).
Hoover, A. E., F. B. Canfield, R. Kobayashi, and T. W. Leland, "Determination of Virial Coefficients by the Burnett Method," *J. Chem. Eng. Data*, **9**, No. 4, 568 (1964).
Kell, G. S., G. E. McLaurin, and E. Whalley, "Second Virial Coefficient of Helium from 0 to 500°C by the Two Temperature Expansion Method," *J. Chem. Phys.*, **68**, 2199 (1978).
Knobler, W. H., J. J. M. Beenakker, and H. F. P. Knapp, "The Second Virial Coefficient of Gaseous Mixtures at 90°K," *Physica*, 25 909 (1959).
Kuenen, J. P., and W. W. Randall, "The Expansion of Argon and Helium as Compared with that of Air and Hydrogen," *Proc. Roy. Soc. London*, **59**, 60 (1895).
Lee, S. M., P. T. Eubank, and K. R. Hall, "Truncation Errors Associated with the Virial Equation," *J. Fluid Phase Eq.*, **1**, 219 (1978). [Corrigendum for Figure 1: **2**, 315 (1979)].
Levelt-Sengers, J. M. H., M. Klein, and J. S. Gallagher, "Pressure-Volume-Temperature Relationships of Gases; Virial Coefficients," *American Institute of Physics Handbook*, 3rd ed., ed., D. E. Gray, McGraw-Hill Book Co., New York (1972).
Linshits, L. R., I. B. Rodkina, and D. S. Tsiklis, "Measurement of the Compressibilities of CO_2-He Mixtures by Burnett's Method," *Zhur. Fiz. Khim.*, **49**, 2141 (1975).
Mansoorian, H., E. F. Capps, H. L. Gielen, P. T. Eubank, and K. R. Hall, "Compact, Magnetic Recirculating Pump for Wide Range Temperature and Pressure Operation," *Rev. Sci. Instrum.*, *46*, No. 10, 1350 (1975).
Mason, E. A. and T. H. Spurling, "The Virial Equation of State," 269, Pergamon Press, Oxford (1969).
McCormack, K. E., and W. G. Schneider, "Compressibility of Gases at High Temperatures, IV. Carbon Dioxide in the Temperature Range 0°-600°, and Pressures up to 50 Atmospheres," *J. Chem. Phys.*, **18**, No. 9, 1269 (1950).
Michels, A., and C. Michels, "Isotherms of CO_2 between 0° and 150° and Pressures from 16 to 250 Atm (Amagat Densities 18-206)," *Proc. Roy. Soc. London*, **A153**, 201 (1935).
Pak, N., and S. Schultz, "Determination of Mixing Effects in a CO_2-He Gas Mixture with a Modified Burnett Apparatus," *Chem. Ing. Tech.*, **50**, No. 11, 889 (1978).
Pfefferle, Jr., W. C., J. A. Goff, and J. G. Miller, "Compressibility of Gases I. The Burnett Method. An Improved Method of Treatment of the Data. Extension of the Method to Gas Mixtures," *J. Chem. Phys.*, **23**, No. 3, 509 (1955).
Pitzer, K. S., and R. F. Curl, Jr., "Empirical Equation for the Second Virial Coefficient," *J. Amer. Chem. Soc.*, **79**, 2369 (1957).
Pope, G. A., P. Chappelear, and R. Kobayashi, "Analysis of Data Obtained by Isochorically Coupled Burnett Experiments," *Physica*, **57**, 127 (1972).
Prausnitz, J. M., *Molecular Thermodynamics of Fluid-Phase Equilibria*, Englewood Cliffs, NJ (1969).
Rayleigh, L., "IX. On the Compressibility of Gases Between One Atmosphere and Half an Atmosphere of Pressure," *Philos. Trans. Roy. Soc. London*, **A204**, 351 (1905).
Reid, R. C., J. M. Prausnitz, and T. K. Sherwood, *The Properties of Gases and Liquids*, 3rd ed., McGraw-Hill, N.J. (1977).
Tsonopoulos, C., "An Empirical Correlation of Second Virial Coefficients," *AIChE J.*, **20**, 263 (1974).
Vennix, A. J., "Low Temperature Volumetric Properties and Development of an Equation of State for Methane," Ph.D. Dissertation, Rice Univ., Houston, TX (1965).
Vukalovich, M. P., and V. V. Altunin, *Thermophysical Properties of Carbon Dioxide*, Collet's Ltd., London (1968).
Watson, M. Q., "The Interaction Second Virial Coefficient for the He-CO_2 System between 230 and 300 K," M.S. Thesis, Texas A&M Univ., College Station, TX (1978).
Waxman, M., H. A. Davis, and J. R. Hastings, "A New Determination of the Second Virial Coefficient of Carbon Dioxide at Temperatures between 0° and 150°C and an Evaluation of its Reliability," *6th Symp. Thermophys. Prop.*, Atlanta (1973).
Weber, L. A., "Thermodynamic and Related Properties of O_2 from the Triple Point to 300 K at Pressures to 330 atm," *NBS Rept.*, **9710** (1968).
Weems, G. W., and M. L. Miller, "Compressibility Factors for Helium and Carbon Dioxide Mixtures at 0 Degrees, 10 Degrees, 20 Degrees, 23 Degrees and 35 Degrees C and up to 900 psia," *U.S. Bur. Mines Rept. Inv.*, **7233** (1969).
Weems, G. W., and A. R. Howard, "Compressibility Factors for Helium and Carbon Dioxide Mixtures at −10 Degrees and −20 Degrees C and Pressures to 1,000 psia," *U.S. Bur. Mine Rept. Inv.*, **7412** (1970).
White, D., T. Rubin, P. Camky, and H. L. Johnston, "The Virial Coefficients of Helium from 20 to 300 Degrees K," *J. Phys. Chem.*, **64**, No. 11, 1607 (1960).
Young, J. G., "Interaction Second Virial Coefficients for C_2H_6-CO_2 System between 250 and 300 K," M.S. Thesis, Texas A&M Univ., College Station, TX (1978).

Manuscript received October 12, 1979; revision received April 4 and accepted May 13, 1980.

Modeling Pulverized Coal Conversion in Entrained Flows

A detailed description of pulverized coal conversion in one-dimensional entrained flows has been formulated and correlated to hydrogasification data from the Rockwell International Flash Hydropyrolysis (FHP) reactor using bituminous coals. This analysis contains physical and chemical descriptions which have not been included in previous mathematical models. These descriptions provide further important insights into the nature of entrained flow coal gasification.

K. M. SPROUSE

Energy Systems Group
Rockwell International
Canoga Park, CA 91304

SCOPE

Entrained flow reactors are increasingly becoming an important concept in the processing of coal into synthetic fuels and thermal energy for power generation. This is primarily due to the fact that entrained flow reactor concepts generally produce faster coal gasification rates (through increased coal-gas surface areas which reduce diffusional resistances) and have a greater ease of operability than fluidized or fixed bed reactors operating at the same coal-firing rates.

Currently, at least two entrained flow coal reactors are commercially available, with another ten in the early development to pilot plant stages for a number of gasification and combustion operating regimes. With this interest in entrained flow coal conversion, it is imperative that the chemical kinetics and hydrodynamics of such reactors be well understood.

The efforts of earlier workers in entrained flow reactor modeling have been described and summarized by Field et al. (1967). These early models basically analyzed the reactor's hydrodynamics as one-dimensional plug flow. When initial mixing processes of the reactants become important, these models can be simply modified to account for mixing by treating the mixing zone as a well stirred tank or by the inclusion of empirical mixing relations. Recently, Wen and Chaung (1979) have used the stirred tank plug flow model with success in simulating the Texaco downflow pilot plant gasifier, while Ubhayaker et al. (1977) and Smoot et al. (1977) have employed empirical mixing relationships with one-dimensional flow for modeling their respective reactor systems.

One-dimensional entrained flow models can pose serious limitations for use as scaling tools in commercial reactor development programs due to their failure in adequately addressing nonuniform flow fields. For reactors in which mixing is achieved predominately by means of recirculation, swirl, or viscous entrainment, it is probably best to consider multidimensional models. One such model is currently being developed by Blake et al. (1979) for three-dimensional transient flows in reactors of any geometry. This model is numerically quite complex employing mixed finite element/finite difference descriptions.

The present study describes, from first principles, the detailed analytical model used in simulating the Rockwell International FHP entrained flow reactor. The analysis assumes one-dimensional plug flow throughout the reactor, an assumption based on the findings of Oberg et. al. (1977) for reactors with impinging-type injectors as used by Rockwell. The one-dimensional reactor dynamic descriptions have been expanded from those of previous models. Of particular importance is the analysis concerning the transport of mass and energy through the gaseous boundary layer surrounding a coal particle. The boundary layer conservation equations are solved in a closed form manner providing algebraic equations for the determination of gas composition at the particle's surface and particle temperature as a function of freestream conditions and internal particle chemistry. Previously, most models assumed the gas composition and temperature at the particle's surface simply to be the same as local freestream conditions.

The analytical model described here is capable, in the general sense, of simulating reactor performance (for those reactors utilizing rapid mixing injection techniques) over a number of gasification regimes. Entrained flow reactor operating regimes of interest today include synthesis gas generation from partial oxidation, hydrogasification, hydroliquefaction, and coal combustion. However, in the present study, this model was only correlated with hydrogasification reactor data. Extending this model to the other gasification regimes will require further analytical development concerning coal particle and freestream gas chemistry.

CONCLUSIONS AND SIGNIFICANCE

Data taken from actual hydrogasification entrained flow reactor experiments with bituminous coals have shown excellent agreement with results predicted by the entrained flow analysis developed here. Measured and predicted values for moisture ash free coal gasified, carbon gasified, reactor exit gas temperature, and reactor exit gas composition were correlated over a range of hydrogasification operating conditions. However, similar attempts to correlate this model with hydrogasification data from subbituminous coals have proved unsuccessful. This result is not surprising considering the coal chemistry analysis employed in this study was developed from an earlier model used by Anthony et al.(1976) for correlating bituminous coal data. The fundamental problem of this coal chemistry formulation as it applies to subbituminous coals, is in its inclusion of coal conversion dependency on total system pressure, a dependency not seen in the lower rank coals.

After fitting to integral reactor experimental data, this model allowed inferences to be made concerning coal particle surface conditions. For example, the model predicted that gas composition at the coal particle's surface (for particle diameters on the order of 50 μm) is nearly the same as the surrounding freestream during all stages of devolatilization and hydrogasification. This prediction is consistent with the assumption made in many entrained flow reactor studies using small pulverized coal particles; whereby, the gas composition at the particle's surface is simply assumed equal to that of the freestream gas. However, the model also predicted that particle temperatures can exceed the surrounding gas freestream temperature by as much as 300°K during some stages of particle hydrogenation due to the exothermic nature of this reaction. This result is significant in that many studies additionally assume particle and freestream gas temperatures equal. Such an assumption according to the model would substantially lower the predicted devolatilization and gasification rates found in this study.

The development of the entrained flow reactor model described here represents a significant effort in the detailed analysis and understanding of such reactor systems. Descriptions for the many physical and chemical processes involved in entrained flow reactors have been combined, providing a systematic analysis based on first principals and the previous efforts of coal researchers. The model is capable of easily being adapted to other regimes of entrained flow pulverized coal conversion such as liquefaction and combustion, as well as being able to handle newer coal chemistry schemes as they become available. Such a model should greatly aid experimental programs in the development of entrained flow pulverized coal reactors.

INTRODUCTION

As research and development continues in the various fields of coal conversion, particularly for the commercialization of entrained flow reactors, theoretical analyses will need to assume greater responsibility in the directing of these experimental programs. This responsibility is extremely important as these reactors begin the scale-up process from bench scale to process development unit (PDU) to pilot plant, and finally to a full-scale commercial plant. Without the use of any detailed reactor model, a fundamental understanding of the dynamic processes and interactions taking place inside the reactor will not be known. If these fundamentals are not well understood, it can probably be expected that the cost and length of any experimental program will be increased and that the final success of obtaining a commercial plant will be diminished.

The analyses and discussions which follow are an attempt to incorporate most of the known dynamic and chemical processes which would be involved in any detailed one-dimensional de-

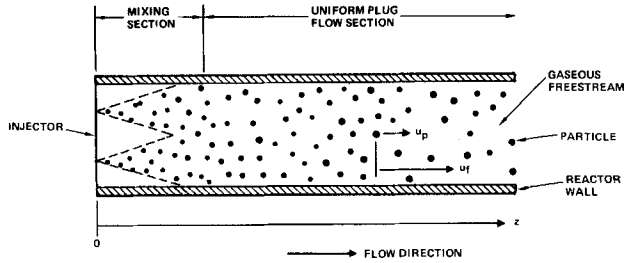

Figure 1. Simplified schematic of flow field inside an entrained flow reactor.

scription of pulverized coal entrained flow reactors. These formulations will basically be divided into two major areas: (1) those primarily concerned with entrained flow reactor dynamics; and (2) those primarily concerned with the chemistry of coal conversion processes within the confines of the coal particle. The first area, entrained flow reactor dynamics, will encompass the physical and chemical descriptions common to entrained flow coal reactors regardless of whether their function is gasification, liquefaction, or combustion. The second area, chemistry of coal conversion processes, will deal primarily with those descriptions belonging only to coal particle chemistry itself; for this treatise, devolatilization and hydrogasification of bituminous coals in particular.

ENTRAINED FLOW REACTOR DYNAMICS

Any entrained flow reactor concept is basically concerned with dispersing small condensed particles (here, the word particle can refer to either the solid or liquid state) into a gaseous medium. Usually this gaseous medium is moving with enough velocity to that its momentum can continually keep the injected particles entrained. The idea behind this entrainment concept is to provide the largest solid-gas (or liquid-gas) surface area possible; thereby reducing diffusional resistances, so that chemical interactions between these phases are more rapid. In this way, chemical reaction times are shortened which means that reactor volumes, utilizing the same reactant flow rates, can also be reduced. This is extremely important economically for high pressure reactors, where any reduction in size can substantially reduce capital equipment costs.

From a simplified viewpoint, the two-phase flow inside an entrained flow reactor can be pictured as being composed of two regimes, one dominated by particle-gas mixing, and the other by uniform plug flow as shown in Figure 1. A one-dimensional coordinate system is placed on the reactor so that its axial direction coincides with the z-axis and its injector is located at $z = 0$. At any location inside the reactor, a particle's velocity is denoted by u_p and the freestream velocity by u_f. Inside the mixing section, the flow field will be predominantly characterized by particle-gas stratification across any plane normal to the z-axis, whereas the uniform plug flow section will be considered to have no such stratification.

In the analysis to follow the dynamical descriptions of the mixing section will be neglected and the uniform plug section will be considered to extend upstream to the injector, at $z = 0$, thus allowing the entire reactor to be viewed as having complete uniform flow throughout. This simplification is based on the work of Oberg et al. (1977) for impinging type injectors in conjunction with pulverized coal dense phase feeding techniques as used in the Rockwell FHP reactor concept. It was shown in their study that the degree of mixing for these injectors is a direct function of the momentum ratio between the incoming impinging jets within a single injection element. By operating these injection elements at the momentum ratio which maximizes mixing, good penetration of the reactant jets can be assured at the point of collision, thus rapidly producing a uniform mixed spray which expands and fills the reactor chamber.

The one-dimensional nature of the flow field is maintained by using as many injection elements as necessary to prevent significant recirculation between elements. This feature of impinging injectors assures that the one-dimensional flow field of the Rockwell FHP reactor is preserved as these reactors are scaled to larger sizes. Therefore, in describing the entrained flow reactor dynamics, only mathematical formulations for the following physical and chemical phenomena will need to be considered. They are in order of discussion: (1) particle boundary layer transport, (2) conservation equations of the bulk flow, (3) chemical reactions of the freestream, and (4) thermochemical and freestream transport properties.

Particle Boundary Layer Transport

Any particle that is placed within a gaseous medium, whereby that particle is either pyrolyzing or at a temperature other than that of the gas which surrounds it, will experience a boundary layer effect. That is, temperature and gas composition at the particle's surface will be different from that of the overall gaseous medium. The purpose of this section is to quantitatively understand how this boundary layer and its associated transport processes will influence gas composition and temperature between the particle's surface and surrounding gas. This is accomplished by writing the equations of mass, momentum, and energy conservation as well as the diffusion equation for the gas inside the boundary layer surrounding the particle.

The solution to these conservation equations in the past have basically evolved into three forms. They categorically are: (1) the vaporization approach, (2) the thin flame surface approach, and (3) the kinetic diffusion approach. All of these forms make use of the steady-state or quasisteady-state assumption whereby time derivatives of the dependent variables found in these equations equal zero. The basic differences among the three solutions are as follows.

The vaporization approach, as first used by such researchers as El Wakil (1956), further assumes that homogeneous chemical reactions do not occur within the boundary layer. On the other hand, the thin flame surface approach, as classically shown by Williams (1965) for burning fuel droplets, allows chemical reactions to occur within the boundary layer, but assumes that their kinetic rates are so fast that a spherical flame surface, burning at stoichiometric conditions, surrounds the particle. Finally, in the kinetic diffusion approach, as used by Axworthy et al. (1976), or Caram and Amundson (1977) for carbon particles, the finite chemical kinetic rates for the production or destruction of gaseous species within the boundary layer are used. In this way, the restrictive assumptions of vaporization or infinite kinetics are removed at the expense of a more complex solution technique.

In regard to entrained flow reactors, where the particles are constantly subjected to convective gas flow over their surface, it has been found best to treat the boundary layer transport process from a vaporization point of view. Combs (1972) explains this reasoning in light of the fact that exposing a pyrolyzing particle to even mild forced convection is likely to blow any flame or chemical reaction surrounding that particle into its wake or even extinguish it. In this way, flame-enhancement of boundary layer transport is not likely to occur for particles traveling in bulk turbulent flow fields. Previously, this reasoning has enjoyed such success in predicting droplet vaporization or combustion rates in convective flows that this vaporization approach is used in the JANNAF (Joint Army, Navy, NASA, Air Force) methodology of analyzing liquid rocket engine combustor performance (see Combs, 1972, and Schuman and Beshore, 1978). Therefore, given the arguments presented above, an analysis for particle boundary layer transport in entrained flows will be developed along the lines of the vaporization analogy. This analysis begins as follows.

Consider a spherical particle surrounded by a gas undergoing pyrolysis or heat exchange as shown in Figure 2. A spherical coordinate system is placed on the particle so that the radial

direction, r, extends from the particle's center outward into the gaseous boundary layer and freestream. The particle's center is given as $r = 0$, and its surface is located at $r = r_s$. Although most particles are not spherical, this description is not altogether in error since it has been found to predict results to problems of a similar nature with excellent accuracy.

The generalized set of conservation equations describing the dynamics of any multicomponent system can be found in many theoretical books on transport processes. In applying these generalized equations to those of mass, momentum, energy, and diffusion through the particle's boundary layer, a few simplifying assumptions will be introduced, thus reducing the complexities of their mathematical solution technique. These assumptions are given as follows.

(a) The system of equations describing flow in the boundary layer will be considered as quasisteady-state.
(b) The boundary layer transport process is one-dimensional in the r-direction (only gradients in r exist).
(c) All body forces are negligible.
(d) The square of the Mach number relative to the particle is much less than unity.
(e) Viscous effects are negligible.
(f) Gaseous radiation is negligible.
(g) The Soret and Dufour effects (thermal diffusion) are negligible.
(h) Pressure gradient diffusion is negligible.
(i) All binary diffusion coefficient pairs will be considered equal.
(j) The Lewis number equals one.
(k) Chemical reactions within the boundary layer are negligible.

The validity of these assumptions, except for Assumption (k) which has already been discussed, will not be expounded here. Assumptions (a) through (j) traditionally belong to a particular class of problem formulation (viz., the Shvab-Zeldovich, see Williams, 1965), which has been thoroughly explained throughout the literature.

Using this set of assumptions, Williams (1965) has shown that the set of conservation equations describing the boundary layer transport processes can be formulated into two governing differential equations, one for species mass fraction, Y_i, and the other for temperature. The equation for species mass fraction is:

$$\frac{d\left[r^2\left(\rho v\, Y_i - \frac{\lambda}{c_p}\frac{dY_i}{dr}\right)\right]}{dr} = 0 \tag{1}$$

and the one for temperature is:

$$\frac{d\left[r^2\left(\rho v \int_{T^o}^{T} c_p\, dT - \frac{\lambda}{c_p}\frac{d\int_{T^o}^{T} c_p\, dT}{dr}\right)\right]}{dr} = 0 \tag{2}$$

In Eqs. 1 and 2, the velocity, v, is the mass averaged species velocity through the boundary layer relative to the particle.

To solve Eqs. 1 and 2, boundary conditions for species mass fraction and temperature will be needed at both the particle surface ($r = r_s$) and freestream (r = infinity). At the particle's surface species diffusion and mass continuity relationships will show that:

$$\left.\frac{\lambda}{c_p}\frac{dY_i}{dr}\right|_{r=r_s} = \frac{\dot{m}_p}{4\pi r_s^2}\, Y_{si} - \frac{\dot{m}_i}{4\pi r_s^2} \tag{3}$$

where $\dot{m}_p$ is the particle mass conversion rate and $\dot{m}_i$ is the species mass flow rate through the boundary layer. By performing an energy balance at the particle's surface, the boundary condition for temperature becomes:

$$\left.4\pi r_s^2 \lambda \frac{dT}{dr}\right|_{r=r_s} = \dot{Q}_{\text{rad}} + \dot{Q}_{\text{reac}} + \frac{4}{3}\pi r_s^3 \rho_p c_{pp}\frac{dT_p}{dt} \tag{4}$$

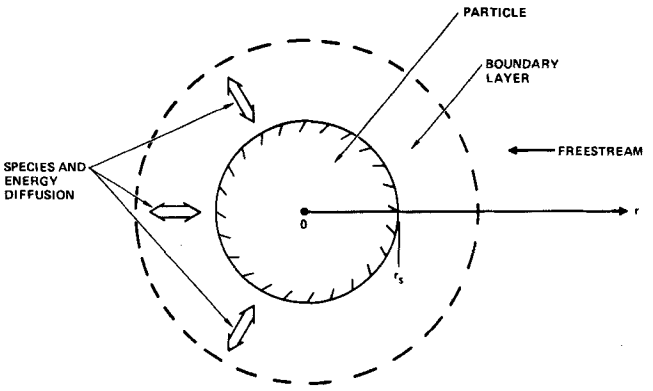

Figure 2. A spherical particle undergoing pyrolysis or heat exchange.

where $\dot{Q}_{\text{rad}}$ is the rate at which heat is radiated away from the particle's surface and $\dot{Q}_{\text{reac}}$ is the rate at which heat is absorbed by the particle due to internal chemical reactions. Endothermic reactions will give positive contributions to $\dot{Q}_{\text{reac}}$, whereas exothermic reactions give negative contributions.

Although this boundary layer development has been assumed to be quasisteady-state, the dT_p/dt term for changes in particle sensible heat was included in Eq. 4, since experience has shown that greater numerical stability in the computer solution for particle temperature can be achieved with this term included in the analysis. Also, Eq. 4 was developed by assuming that temperature gradients within the particle are negligible, thus allowing the temperature at the particle's surface to be given by the particle temperature, T_p. This assumption is usually true for small nonpyrolyzing spheres when the surrounding gas thermal conductivity is much less than that of the spheres themselves, therefore giving rise to extremely small particle Biot moduli. While these particles are decomposing, their Biot moduli are reduced even further due to heat transfer blockage from the freestream to the particle produced by the convective flow of mass away from the particle's surface. The validity of this assumption as it applies to the experimental situation studied in this paper will be further discussed in the experimental results section.

The boundary conditions for species mass fraction and temperature at the freestream (r = infinity) are somewhat simpler than those at the particle's surface. The one for species mass fraction is:

$$Y_i = Y_{fi} \tag{5}$$

whereas the one for temperature is:

$$T = T_f \tag{6}$$

Here, the subscript f denotes freestream conditions.

Solving the boundary value problems now formulated will show that the gaseous species mass fraction at the particle's surface, given by the solution of Eqs. 1, 3, and 5 for multicomponent and countercurrent diffusion, is:

$$Y_{si} = \left(Y_{fi} - \frac{\dot{m}_i}{\dot{m}_p}\right)\exp\left(\frac{-\dot{m}_p c_p}{2\, Nu\, \pi\, r_s \lambda}\right) + \frac{\dot{m}_i}{\dot{m}_p} \tag{7}$$

The change in temperature at the particle's surface is found from the solution to Eqs. 2, 4, and 6 with the result being:

$$\frac{dT_p}{dt} = \frac{3\,\dot{m}_p\, c_p\,(T_p - T_{WB})}{4\,\pi r_s^3 \rho_p\, c_{pp}\left[1 - \exp\left(\frac{\dot{m}_p c_p}{2\, Nu\, \pi r_s \lambda}\right)\right]} \tag{8}$$

Eq. 8 used the particle's wet bulb temperature, T_{WB}, which is defined as the limiting temperature that the particle can achieve under the given set of quasisteady-state conditions. The wet bulb temperature is found by solving Eqs. 2, 4, and 6; only this time, the derivative dT_p/dt in Eq. 4 is set equal to zero. This will produce the result:

$$T_{WB} = T_f + \left[\frac{\dot{Q}_{rad} + \dot{Q}_{reac}}{\dot{m}_p\, c_p}\right]\left[1 - \exp\left(\frac{\dot{m}_p\, c_p}{2\, Nu\, \pi r_s \lambda}\right)\right] \quad (9)$$

The Nusselt number, Nu, has been included in Eqs. 7 through 9, since it is known that the ratio of mass flow rates for a vaporizing or burning particle under stagnant to convective atmospheric conditions is equal to Nu divided by 2.0. (See Williams, 1965.)

Eqs. 7 through 9 provide a more detailed picture as to the nature of the gas composition and temperature at the particle's surface in relation to freestream values. In most analyses concerning entrained flow coal gasification, it is usually assumed, since the coal particle is extremely small, that the gas composition and temperature at the particle's surface are the same as in the freestream. Practice has shown that in many circumstances this assumption is not valid, particularly during stages of rapid particle oxidation where particle temperatures have been experimentally found to exceed those of the gaseous freestream by as much as 500°K for particle sizes on the order of 70 μm. (See Smith, 1971.)

Conservation Equations of the Bulk Flow

Determining the amount of change in many reactor parameters from one location to the next will require the solutions to the bulk flow conservation equations for mass, momentum, and energy, as well as the gaseous equation of state and particle-drag relationship. Changes in such parameters as freestream velocity, particle velocity, species flow rates, reactor temperature, etc., will be found from the following analysis. This analysis will utilize the geometrical descriptions of the uniform plug flow section as provided by Figure 1.

In developing the equations governing the reactor's bulk flow, the following simplifying assumptions will be introduced.

(l) The bulk flow processes will be considered as steady-state, one-dimensional, uniform flow.
(m) Viscous effects are negligible.
(n) All body forces are negligible.
(o) Diffusion processes are negligible.
(p) Thermal conduction and radiation are negligible in the axial direction.

Assumption (l) is usually satisfied after sufficient reactor operational times and good injection mixing. However, the validity of Assumptions (m) through (p) as applied to various entrained flow coal reactors will remain to be seen, although they have been shown to yield adequate results for liquid rocket combustor analyses.

Probably the most questionable assumption is the one concerning negligible thermal conduction and radiation in the axial direction, Assumption (p). However, if the mass-average temperature of the initially injected reactant streams is high enough to promote rapid chemical reactions once these streams are mixed, the conduction and radiation of thermal energy upstream from the reaction zone is not required to heat the mixed reactants up to the ignition temperature. Also, if the bulk flow velocity is fast enough that only convective energy flow dominates in the reaction zone, thermal conduction and radiation over the entire reactor's axial direction becomes unimportant.

By performing a species mass balance across any given control volume in the uniform plug flow section of Figure 1 and by using Assumption (l), the following two species conservation equations for gases and freestream condensed phases can be written.

$$\frac{d\dot{n}_i}{dz} = A_g\, \dot{\omega}_i + \sum_j \frac{\dot{N}_j\, \dot{m}_{i,j}}{u_{pj}} \quad (10)$$

and

$$\frac{d\dot{n}_{ci}}{dz} = A_g \dot{\omega}_{ci} \quad (11)$$

Here, $\dot{n}_i$ and $\dot{n}_{ci}$ are the freestream mass flow rates of gaseous and condensed species traveling in the axial direction, whereas $\dot{N}_j$ is the number flow rate of the j^{th} particle group.

Eq. 10 simply states that the change in freestream flow rate of the i^{th} gaseous species is equal to the amount of that species produced by homogeneous freestream reactions plus the amount added by particle decomposition of all j particle groups. On the other hand, Eq. 11 states that the change in freestream flow rate of the i^{th} condensed freestream species is equal only to that produced by homogeneous freestream reactions, since condensed phases cannot diffuse through particle boundary layers. It should be noted here that the term "condensed freestream species" refers to any homogeneous condensed phase which is originally formed from gaseous freestream reactions, such as the formation of carbon soot from homogeneous coking reactions. These freestream condensed phases will travel at the same velocity and temperature as the freestream gases.

Overall gas continuity also needs to be included in this set of equations for mass conservation. This equation can be written as:

$$\sum_i \dot{n}_i = \rho_f\, u_f\, A_g \quad (12)$$

where the freestream gas density, ρ_f, can be found from the equation of state.

In Eqs. 10 through 12, the effective cross-sectional area of the total gas flow, A_g, is determined by knowing the total reactor cross-sectional area, A, and the effective areas occupied by condensed freestream species and particles, respectively. Quantitatively, this can be expressed as:

$$A_g = A - \left[\frac{1}{u_f}\sum_i \frac{\dot{n}_{ci}}{\rho_{ci}} + \frac{4\pi}{3}\sum_j \frac{\dot{N}_j\, r_{sj}^3}{u_{pj}}\right] \quad (13)$$

In the following governing equations for overall bulk momentum and energy, the following relation for the mass lost by the j^{th} particle to the mass flow rate through its boundary layer is used.

$$\frac{4\pi}{3}\frac{d(r_{sj}^3\, \rho_{pj})}{dz} = \frac{-\dot{m}_{pj}}{u_{pj}} \quad (14)$$

Eq. 14 is also needed in determining the change in particle radius for the j^{th} particle group.

Now, by again using a control volume in the uniform plug flow section of Figure 1, it can be shown that equating the change in momentum across that volume to the sum of the forces acting upon it will, after employing Assumptions (l) through (n) and Eq. 14, yield a bulk flow momentum equation of:

$$\left(\sum_i \dot{n}_i + \sum_i \dot{n}_{ci}\right)\frac{du_f}{dz} + A\frac{dP}{dz} = \sum_j \dot{N}_j\, \dot{m}_{pj} - \left[\frac{4\pi}{3}\sum_j r_{sj}^3\, \rho_{pj}\, \dot{N}_j \frac{du_{pj}}{dz} + u_f\left(\sum_i \frac{d\dot{n}_i}{dz} + \sum_i \frac{d\dot{n}_{ci}}{dz}\right)\right] \quad (15)$$

Finally, the control volume approach is used one last time for the development of the bulk flow energy equation. Using Assumptions (l) through (p) and Eq. 14, an energy balance on the control volume will show that:

$$u_f\left(\sum_i \dot{n}_i + \sum_i \dot{n}_{ci}\right)\frac{du_f}{dz} + \left(\sum_i \dot{n}_i\, c_{pi} + \sum_i \dot{n}_{ci}\, c_{pci}\right)\frac{dT_f}{dz} = \sum_j \left(h_{pj} + \frac{u_{pj}^2}{2}\right)\frac{\dot{N}_j\, \dot{m}_{pj}}{u_{pj}} - \left[\frac{4\pi}{3}\sum_j r_{sj}^3\, \rho_{pj}\, \dot{N}_j\left(c_{ppj}\frac{dT_{pj}}{dz} + u_{pj}\frac{du_{pj}}{dz}\right) + \sum_i \left(h_i + \frac{u_f^2}{2}\right)\frac{d\dot{n}_i}{dz} + \sum_i \left(h_{ci} + \frac{u_f^2}{2}\right)\right.$$

$$\frac{d\dot{n}_{ci}}{dz} + \frac{d\dot{Q}_{out}}{dz}\Bigg] \quad (16)$$

where $\dot{Q}_{out}$ is the rate of energy conducted through the reactor walls and out of the system.

For low speed flows, specifically *where* $u_f^2/(P/\rho_f) << 1.0$, Eqs. 15 and 16 can be greatly simplified. Eq. 15 would simply state, for momentum, that pressure is constant, while Eq. 16 could be reduced by the elimination of all kinetic energy terms. However, these equations were written in this longer format because some reactors, such as coal-fired combustors for magnetohydrodynamic (MHD) power generation, can have internal gas velocities approaching Mach numbers of unity.

In completing the physical descriptions of the bulk flow, one final equation for particle-drag needs to be written. By equating the force exerted on a particle by the freestream gas to the particle's mass times acceleration, the following equation of change for particle velocity can be given as:

$$\frac{du_{pj}}{dt} = \frac{3\, C_{Dj}|u_f - u_{pj}|(u_f - u_{pj})\, \rho_f}{8\, r_{sj}\rho_{pj}} \quad (17)$$

It has been shown by Abraham (1970) that the drag coefficient for spheres, C_D, over a wide range of Reynolds numbers (i.e., $0 \leq Re \leq 5000$) can be best correlated by the relation:

$$C_{Dj} = \frac{24}{Re_j}(1 + 0.1104\sqrt{Re_j})^2 \quad (18)$$

In relating the time rate of change of various particle parameters, such as u_{pj} in Eq. 17 and T_p in Eq. 8, to the axial rate of change, the dt terms in these equations (as well as others to be developed later) should be replaced by dz/u_{pj}.

Chemical Reactions of the Freestream

The mass species production rates, $\dot{\omega}_i$ and $\dot{\omega}_{ci}$, found in Eqs. 10 and 11 can be directly determined from homogeneous kinetic reaction data among the various gaseous freestream species. This is accomplished by knowing the basic series of reaction steps or chemical equations involved in the overall reaction process. For example, a generalized equation for the k^{th} homogeneous kinetic reaction step, can be expressed as:

$$\sum_i \nu'_{i,k} Z_i \xrightarrow{k_k} \sum_i \nu''_{i,k} Z_i + \sum_i \nu''_{ci,k} Z_{ci} \quad (19)$$

In this equation, ν' and ν'' denote the stoichiometric coefficients for reactants and products with the symbol Z representing the chemical formula of a given compound. The subscript k denotes a given kinetic reaction step. It should be noted from Eq. 19 that condensed freestream species, given by the subscript c, do not appear as reactants.

Now, from kinetic theory and the system of chemical reactions given by Eq. 19, the homogeneous mass production rate of the i^{th} gaseous species is given by:

$$\dot{\omega}_i = M_i \sum_k (\nu''_{i,k} - \nu'_{i,k})\, k_k \prod_i \left(\frac{\rho_f Y_{fi}}{M_i}\right)^{\nu'i,k} \quad (20)$$

whereas, for the i^{th} condensed freestream species, the mass production rate is given by:

$$\dot{\omega}_{ci} = M_{ci} \sum_k \nu''_{ci,k} k_k \prod_i \left(\frac{\rho_f Y_{fi}}{M_i}\right)^{\nu'i,k} \quad (21)$$

In Eqs. 19 through 21, the homogeneous specific reaction rate constant, k_k, is given by an Arrhenius rate expression.

Many times a complete set of reaction rate data for the production of various chemical species is not well known or there are so many reaction steps involved that the determination of these production rates becomes a costly and time-consuming task. However, if the freestream temperature is sufficiently high causing the reaction rates to be extremely rapid, it can be assumed that the finite kinetic schemes given by Eqs. 19 through 21 can be replaced by a chemical equilibrium analysis.

The type of chemical equilibrium analysis employed for entrained flow reactors is given by a constant pressure process such as those described by Huff et al. (1951) or Gordon and McBride (1971). Therefore, by knowing the instantaneous changes in freestream enthalpy and atomic flow rates across the control volume, the rate of change of freestream species flow rates can then be determined. Once equilibrium has been solved for changes in freestream species flow rates, the two species production rates can then be determined from:

$$\dot{\omega}_i = \frac{1}{A_g}\left[\left.\frac{d\dot{n}_i}{dz}\right|_{eq} - \sum_j \frac{\dot{N}_j\, \dot{m}_{i,j}}{u_{pj}}\right] \quad (22)$$

and

$$\dot{\omega}_{ci} = \frac{1}{A_g}\left.\frac{d\dot{n}_{ci}}{dz}\right|_{eq} \quad (23)$$

where the subscript eq in these two equations means evaluated from chemical equilibrium.

An equilibrium development for obtaining the $d\dot{n}_i/dz|_{eq}$ and $d\dot{n}_{ci}/dz|_{eq}$ terms will not be given here since complete derivations for chemical equilibria, such as those by Huff et al. (1951), and Gordon and McBride (1971), do exist in literature and are quite lengthy in volume to be merely repeated in this discussion.

Thermo-Chemical and Freestream Transport Properties

The thermo-chemical properties used in this model for gaseous and condensed species were taken from the tables compiled by Stull and Prophet (1971). These tables have been curve fitted by Gordon and McBride (1971) for species specific heat, enthalpy, and entropy. The transport properties for dynamic viscosity and thermal conductivity of gas mixtures were calculated from kinetic theory as given by Hirschfelder et al. (1954). A complete listing of the values to be used for the force constants in these equations has been compiled by Svehla (1962) for most gases at elevated temperatures.

CHEMISTRY OF COAL PARTICLE DEVOLATILIZATION AND HYDROGASIFICATION

With the completion of the analytical formulations in the first major area (entrained flow reactor dynamics), attention can now be directed towards developing an analysis for the second major area on chemistry of coal conversion processes within the confines of the coal particle itself. Since this reactor study was concerned only with entrained flow hydrogasification, the following coal conversion chemical processes will reflect only those areas relating directly to devolatilization and hydrogasification. That is, coal particle chemistry for liquefaction or other gasification regimes will not be considered here.

Coal particle chemistry of devolatilization and hydrogasification is far from being thoroughly understood. Numerous mechanisms have been proposed by which coal decomposes in inert and hydrogen atmospheres. However, each of these proposed mechanisms has various shortcomings and more fundamental research is needed. The journal review article of Anthony and Howard (1976) describes much of this previous work.

Even though the exact chemistry of coal devolatilization and hydrogasification is not complete, an analytical formulation based on current research was developed to couple with the previous descriptions of the entrained flow reactor dynamics. Two of the most promising treatises considered for incorporation into this work were those given by Johnson (1977) and Anthony et al. (1976). After further examination, it was decided to use the approach of Anthony et al. (1976), since they considered hydrogasification reactions to occur within and at the coal particle's surface during the initial onset of devolatilization, whereas Johnson's approach did not. For the entrained flow model developed here which considers boundary layer trans-

port, hydrogen appears at the coal particle's surface throughout most of devolatilization at concentrations very near those in the freestream. Therefore, the analysis to be used, similar to that presented by Anthony et al. will be developed as follows.

Consider only four types of gaseous species which can diffuse through the boundary layer surrounding the coal particle. These four gaseous species are classified as reactive volatiles, nonreactive volatiles, hydrogenated volatiles, and hydrogen. Reactive volatiles are high molecular weight hydrocarbons, which once formed by particle pyrolysis can: (a) react with hydrogen, forming hydrogenated volatiles; (b) deposit themselves back onto the coal particle through deposition reactions; or (c) diffuse through the boundary layer escaping out into the freestream. Thus, the mass flow rate of reactive volatiles, $\dot{m}_{rv}$, through the boundary layer can be expressed as:

$$\dot{m}_{rv} = \frac{dV_{rv}}{dt} - \rho_{s_{rv}}(k_1 + k_2 P_{s_{H_2}}) \tag{24}$$

Now, nonreactive volatiles are lower molecular weight hydrocarbons, which once formed by particle pyrolysis are able to diffuse away from the coal particle and into the freestream without being subjected to the secondary reactions of deposition and hydrogenation encountered by reactive volatiles. Thus, the mass flow rate of nonreactive volatiles, $\dot{m}_{nrv}$, through the boundary layer is simply given by:

$$\dot{m}_{nrv} = \frac{dV_{nrv}}{dt} \tag{25}$$

On the other hand, hydrogenated volatiles are formed either by homogeneous pore reactions of hydrogen with reactive volatiles, or by heterogeneous surface reactions of hydrogen with the solid coal matrix. The amount of hydrogenated volatiles liberated by heterogeneous surface reactions is assumed by Anthony to be directly proportional to the fractional completion of reactive volatiles formation, for any hydrogen concentration at the particle's surface. This analysis further assumed that for homogeneous hydrogenation reactions, the ratio of hydrogenated volatile mass produced to reactive volatile mass consumed is approximately 5/4, and that for heterogeneous surface reactions the ratio of hydrogenated volatile mass produced to carbon mass consumed is approximately 4/3. These mass ratios were determined from the following two global reactions, respectively:

$$C_{15}H_8O_3(g) + 29\ H_2(g) \rightarrow 15\ CH_4(g) + 3\ H_2O(g)$$

and

$$C(s) + 2H_2(g) \rightarrow CH_4(g)$$

where $C_{15}H_8O_3(g)$ has been chosen as a model formula for reactive volatiles, this formula was determined from coal fragment structures proposed by Wender (1975) for various coals. From these assumptions then, the mass flow rate of hydrogenated volatiles, $\dot{m}_{hv}$, through the boundary layer can be given by:

$$\dot{m}_{hv} = P_{s_{H_2}}\left(\frac{5}{4} k_2 \rho_{s_{rv}} + \frac{4k_3}{3V_{rv}^{**}} \frac{dV_{rv}}{dt}\right) \tag{26}$$

Finally, the mass flow rate of hydrogen gas, $\dot{m}_{H_2}$, through the boundary layer is of the same form as Eq. 26 for hydrogenated volatiles, except that the two global expressions for homogeneous and heterogeneous hydrogen reactions dictate that:

$$\dot{m}_{H_2} = -P_{s_{H_2}}\left(\frac{1}{4} k_2 \rho_{s_{rv}} + \frac{k_3}{3V_{rv}^{**}} \frac{dV_{rv}}{dt}\right) \tag{27}$$

Notice that the mass flow rate of hydrogen gas in the particle boundary layer, $\dot{m}_{H_2}$, is negative, since it will always be flowing to the particle's surface.

The devolatilization production terms of nonreacting volatiles, dV_{nrv}/dt, and reacting volatiles, dV_{rv}/dt, found in Eqs. 24 through 27 are directly adapted from the work of Anthony et al. as:

$$\frac{dV_{nrv}}{dt} = W_{\text{coal}}^{o} V^{**} \int_0^{E_1} k_o f(E) \exp\left(\frac{-E}{R_u T_p}\right) \exp\left[-\int_o^t k_o \exp\left(\frac{-E}{R_u T_p}\right) dt\right] dE \tag{28}$$

and

$$\frac{dV_{rv}}{dt} = W_{\text{coal}}^{o} V^{**} \int_{E_1}^{\infty} k_o f(E) \exp\left(\frac{-E}{R_u T_p}\right) \exp\left[-\int_o^t k_o \exp\left(\frac{-E}{R_u T_p}\right) dt\right] dE \tag{29}$$

such that

$$f(E) = (\sigma\sqrt{2\pi})^{-1} \exp\left[\frac{-(E - E_o)^2}{2\sigma^2}\right] \tag{30}$$

It should be noted here that $\int_o^{\infty} f(E)dE = 1$.

The overall rate coefficients, k_1 and k_2, for reactive volatile deposition and homogeneous hydrogenation reactions, found in Eqs. 24, 26, and 27, are given by the following two relations as:

$$k_1 = \frac{4\pi r_s \lambda RT\, c_1}{c_p} \tag{31}$$

and

$$k_2 = \frac{4\pi r_s \lambda RT\, c_2}{c_p} \tag{32}$$

where $c_1$and c_2 are assumed to be constants which are determined from experiment. The constant c_1 is defined as the reacting volatile deposition rate coefficient, k_1, divided by the reacting volatile pressure independent mass transfer coefficient, k_c; the constant c_2 is simply the homogeneous reacting volatile hydrogenation coefficient, k_2, divided by k_c. Eqs. 31 and 32 were determined by first finding an expression for k_c. This was done by assuming in Eq. 7 that $\dot{m}_p = \dot{m}_i$, $Y_{fi} = 0$, $Nu = 2$, Y_{si} is very small, $i = rv$, and then substituting this equation into Anthony et al.'s expression for the reactive volatile boundary layer flow rate of:

$$\dot{m}_{rv} = \frac{k_c}{P} \rho_{s_{rv}}$$

to get

$$k_c = \frac{4\pi r_s \lambda RT}{c_p}$$

where use was made of the perfect gas relationship.

Typical values used for the constants in this section are found in Table 1. These constants, except for the hydrogen-coal heterogeneous reaction rate constant, k_3, and the volatile molecular weights, were taken from the work of Anthony et al. (1976) for bituminous coals. The value reported for k_3 was chosen because it gave the best data correlation for the bituminous coals tested in this study. The values used for molecular weights of the volatiles are simply qualitative estimates: the reactive volatiles being given by the $C_{15}H_8O_3$ model formula previously discussed, nonreactive volatiles given by an average of aromatic molecules from benzene to chrysene, and the molecular weight of hydrogenated volatiles simply given by that of methane. The

TABLE 1. DEVOLATILIZATION AND HYDROGASIFICATION CONSTANTS FOR BITUMINOUS COALS

c_1	=	5.53×10^{-6} Pa^{-1}
c_2	=	1.95×10^{-12} Pa^{-2}
V_{rv}^{**}	=	0.20
V^{**}	=	0.572
k_o	=	1.67×10^{13} s^{-1}
k_3	=	3.4×10^{-8} Pa^{-1}
σ	=	7.2×10^{4} J/mol
E_o	=	2.29×10^{5} J/mol
E_1	=	2.57×10^{5} J/mol
M_{rv}	=	236 g/mol
M_{nrv}	=	178 g/mol
M_{hv}	=	16.0 g/mol

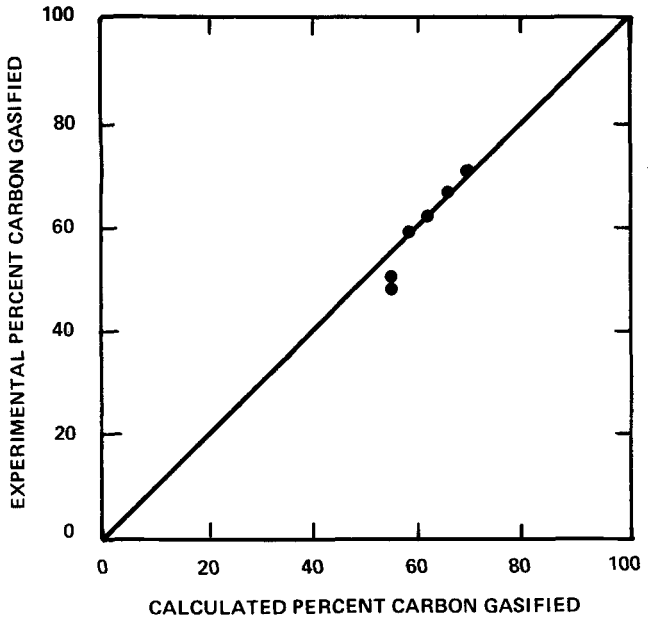

Figure 3. Reactor model calculated vs. experimental carbon conversions for bituminous coal tests.

sensitivity of model results on the exact values chosen for these molecular weights has been seen to be small. This is because these molecular weights are used only in the calculation of hydrogen partial pressure at the particle's surface. Due to the fact that the molecular weight of hydrogen is much smaller than those given in Table 1, it is seen that their influence in hydrogen partial pressure is small.

Should the exact chemical composition of all volatile material diffusing through the particle boundary layer be known, this discussion could be concluded after determining the mass enthalpy of the coal particle, h_p, and $\dot{Q}_{reac}$ needed in equations previously described. However, this is not the case, and before the bulk flow conservation equations already described can be solved, the chemical species leaving the coal particle must be further defined. From the earlier assumption of rapid reaction rates in the freestream, thus allowing changes in freestream species flow rates to be determined directly from chemical equilibrium, the instantaneous changes in atomic flow rates needed for this analysis can be found from data given by Gray et al. (1975) for hydrogasification.

The data given by Gray et al. show the amount of mass converted of the various atomic elements found in coal, as a function of the coal atomic carbon converted during hydrogasification. Using this data the following equations were empirically formulated.

$$\eta_{hyd} = \eta_{nit} = \eta_{ox} = \eta_{car}^{0.201} \tag{33}$$

and

$$\eta_{sul} = \eta_{car}^{0.644} \tag{34}$$

where the fraction of species converted in the coal, η, is given in these two equations on a moisture ash-free (maf) basis. The fraction of water vaporized from the coal particle was assumed to be very rapid in this study and given by the relation:

$$\eta_{H_2O} = \eta_{car}^{0.004} \tag{35}$$

All the ash is assumed to remain on the coal particle throughout hydrogasification, without evaporating into the freestream. Knowing that the particle mass consumption rate, $\dot{m}_p$, is given by:

$$\dot{m}_p = \dot{m}_{rv} + \dot{m}_{nrv} + \dot{m}_{hv} + \dot{m}_{H_2} \tag{36}$$

a continuity balance with the coal constituents will also show that:

TABLE 2. MAIN EQUATIONS AND DEPENDENT VARIABLES

Section	Equations	Variables
Particle Boundary Layer Transport	Eqs. 7 and 8	Y_{sj}, T_P
Conservation Eqs. of Bulk Flow	Eqs. 10-17	$\dot{n}_i$, $\dot{n}_{c_i}$, A_a, P, T_f, u_f, u_{pj}, r_{sj}
Chemical Reactions of Freestream	Eqs. 22 and 23	$\dot{\omega}_i$, $\dot{\omega}_{ci}$
Thermo-Chemical and Freestream Transport Properties	Gordon and McBride (1971)	c_{p_i}, c_{pc_i}, h_i, h_{c_i}
	Hirschfelder et al. (1954)	μ, λ
Chemistry of Coal Particle Devolatilization and Hydrogasification	Eqs. 24-27 and 36	$\dot{m}_{rv}$, $\dot{m}_{nrv}$, $\dot{m}_{hv}$, $\dot{m}_{H_2}$ $\dot{m}_p$
	Eqs. 33-35 and 39	η_{hyd}, η_{nit}, η_{ox}, η_{sul}, η_{H_2O}, η_{car}
	Eq. 40	h_p

$$\dot{m}_p = W^o_{coal}\left(\eta^o_{car}\frac{d\eta_{car}}{dt} + \eta^o_{hyd}\frac{d\eta_{hyd}}{dt} + \eta^o_{ox}\frac{d\eta_{ox}}{dt} + \eta^o_{nit}\frac{d\eta_{nit}}{dt} + \eta^o_{sul}\frac{d\eta_{sul}}{dt} + \eta^o_{H_2O}\frac{d\eta_{H_2O}}{dt}\right) \tag{37}$$

where the initial mass fraction of a given constituent in the coal, η^o, is given here on an as-received basis. For completeness, it should be stated in this study that:

$$\eta^o_{car} + \eta^o_{hyd} + \eta^o_{ox} + \eta^o_{nit} + \eta^o_{sul} + \eta^o_{H_2O} + \eta^o_{ash} = 1.0 \tag{38}$$

Now by substituting Eqs. 33 through 35 into Eq. 37, the rate at which atomic carbon is converted can be found directly from the particle mass consumption rate, $\dot{m}_p$. This equation is given by:

$$\frac{d\eta_{car}}{dt}\left[\eta^o_{car} + 0.201\ \eta^{-0.799}_{car}\left(\eta^o_{hyd} + \eta^o_{ox} + \eta^o_{nit}\right) + 0.644\ \eta^o_{sul}\,\eta^{-0.356}_{car} + 0.004\ \eta^o_{H_2O}\,\eta^{-0.996}_{car}\right] = \frac{\dot{m}_p}{W^o_{coal}} \tag{39}$$

where $\dot{m}_p$ is determined from Eq. 36.

In completing the chemical descriptions of a decomposing coal particle under devolatilization and hydrogasification conditions, the mass enthalpy of the coal particle must be determined. Since it has already been assumed that the ash material does not enter the freestream but remains with the leftover char, the mass enthalpy of the particle, h_p, is determined on an ash-free basis. If it is assumed that the mass specific heat of the ash free coal particle is very near that of the ash itself and constant, the following equation for h_p can be expressed as:

$$h_p = h^o_{afc} + c_{pp}\,(T - T^o) \tag{40}$$

The mass enthalpy of formation of the ash-free coal, h^o_{afc}, can be determined from the coal's ultimate analysis and heat of combustion on an as-received basis. By assuming complete oxidation of the as-received coal and treating the ash material as inert during the combustion of coal with oxygen, the mass enthalpy of formation of the ash-free coal can be given by:

$$h^o_{afc} = \frac{1}{(1 - \eta^o_{ash})}\left[\Delta H_{coal} + \frac{\eta^o_{car}\,M_{CO_2}h^o_{CO_2}}{M_{car}} + \left(\frac{\eta^o_{hyd}\,M_{H_2O}}{2M_{hyd}} + \eta^o_{H_2O}\right)h^o_{c_{H_2O}} + \frac{\eta^o_{sul}\,M_{SO_2}\,h^o_{SO_2}}{M_{sul}}\right] \tag{41}$$

where ΔH_{coal} is the higher heat of combustion per unit mass of coal on an as-received basis at reference temperature, T^o. The reference temperature, T^o, in Eq. 41 is usually taken to be 298°K, so that any water that is formed will generally be in the liquid state. Therefore, the enthalpy of formation of water,

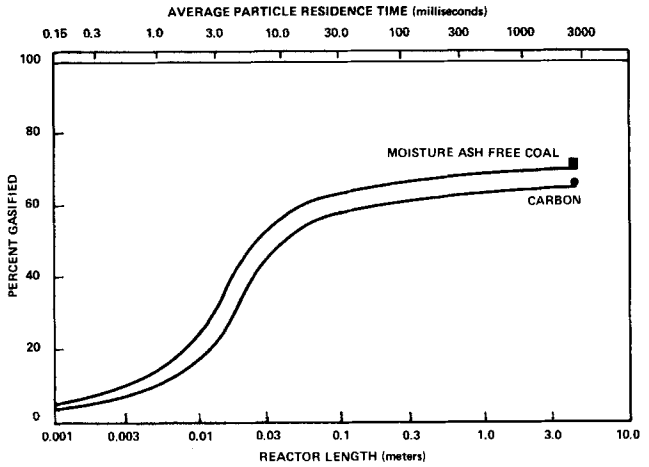

Figure 4. Reactor gasification model predictions for a bituminous coal test.

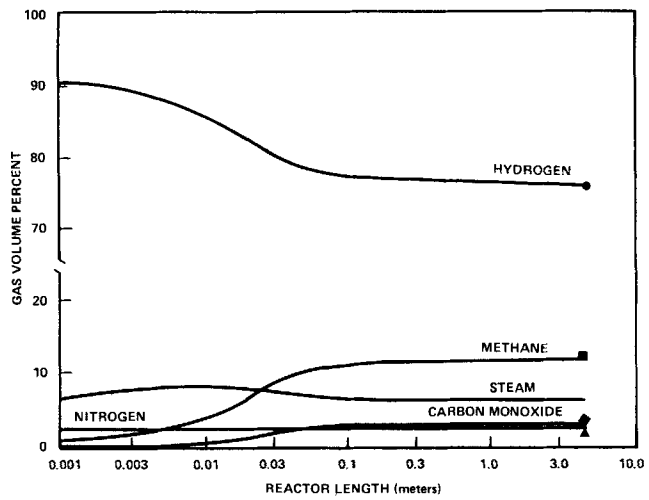

Figure 6. Reactor gas composition model predictions for a bituminous coal test.

$h^o_{cH_2O}$, in that equation must be given for the liquid phase with ΔH_{coal} equivalent to the higher heat of combustion. Enthalpies of formation for oxygen and nitrogen molecules were not included since at the reference temperature, T^o, they are generally defined as zero (Stull and Prophet, 1971).

The rate of heat absorbed by internal coal particle reactions, $\dot{Q}_{reac}$, was given for this study simply by the reaction $C(s) + 2H_2(g) \rightarrow CH_4(g)$, which produces a heat of reaction of approximately -1.87×10^7 J/kg of hydrogen consumed by the coal particle. Therefore, $\dot{Q}_{reac}$ is simply this heat of reaction times the hydrogen consumption rate. The negative number for the heat of reaction with hydrogen indicates by convention that this reaction is exothermic.

SOLUTION METHODOLOGY

The main body of 30 equations to be solved and their 30 dependent variables are listed in Table 2. These main equations together with a few other relationships, such as the gas equation of state and some simple continuity expressions required as input for the determination of $\dot{\omega}_i$ and $\dot{\omega}_{ci}$ from chemical equilibrium, constitute the complete description for this entrained flow analysis. This set of linear and nonlinear equations was solved in a finite difference computing scheme. Since all differential equations found in this set are simple ordinary-first-order, only one boundary condition is required for each differential equation at the upstream location. Therefore, the numerical iteration solution begins at the injection plane, $z = 0$, where all dependent variables are initialized, and then simply marches down the reactor's axial length one step at a time. The distance between axial steps is denoted by Δz.

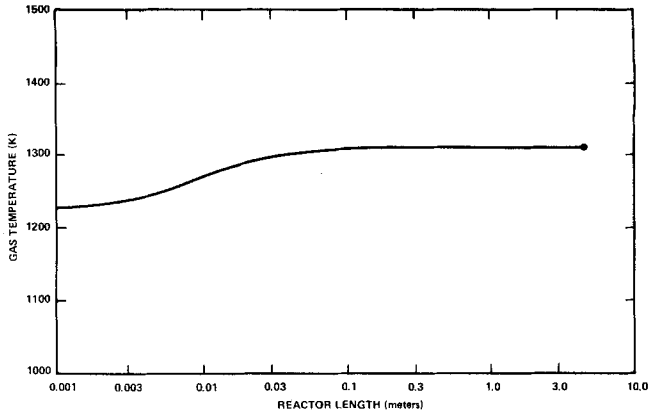

Figure 5. Reactor gas temperature model prediction for a bituminous coal test.

EXPERIMENTAL RESULTS

These analytical formulations were correlated against actual entrained flow reactor tests performed by Rockwell International with bituminous coals in an adiabatic reactor (Friedman, 1979). Two types of bituminous coals were tested, a Kentucky No. 9 hvAb (Island Creek), and an Illinois No. 6 hvCb coal. The proximate analysis of these coals (as tested) was 5.52% moisture, 36.19% volatile matter, 49.92% fixed carbon, and 8.37% ash for the Kentucky coal, with 6.48% moisture, 34.03% volatile matter, 50.32% fixed carbon, and 9.17% ash for the Illinois coal. Keeping a fairly constant coal flow rate to the reactor of 0.05 kg/s for all tests, the reactor operating conditions were varied across the following parameter ranges. Pressure was varied from 6.8 to 10.3 MPa, gas-particle residence time varied from 0.94 to 3.12 s, average reactor temperature was changed from 1,070 to 1,340 K, and the mass ratio of hydrogen to coal was varied from 0.34 to 0.64.

Figure 3 shows a comparison of reactor model calculated and experimental carbon conversions for the bituminous coal tests. As seen from this figure, the computer model calculations agreed quite closely with the actual experimental results. Similar comparisons between model and experiment for moisture ash-free conversion, reactor exit gas temperature, and reactor exit gas composition showed the same type of agreement.

As stated in the hydrogasification coal chemistry section, only Anthony's heterogeneous rate constant, k_3, was changed to obtain good data correlation (its value being increased from 0.010 MPa^{-1} to 0.034 MPa^{-1}). From the Moseley and Paterson view on heterogeneous gasification as developed by Anthony and Howard (1976), this change would mean that the coals tested in this study produced more active sites for hydrogenation during devolatilization than did Anthony's Pittsburgh Seam No. 8 high-volatile bituminous coal.

As an example of the type of information which can be obtained from such an entrained flow hydrogasification model, Figures 4 to 6 show plots of various important reactor variables as a function of reactor length. These computer results were based on a test with Kentucky No. 9 hvAb coal where the reactant flowrates for the coal, hydrogen, oxygen, and the coal's transport nitrogen were 0.0525, 0.0255, 0.0124, and 0.0076 kg/s, respectively. The hydrogen was preheated to 798°K and the remaining reactants were fed to the reactor at ambient temperatures. The reactor parameters for this test were a reactor pressure of 10.42 MPa, reactor length of 4.57 m, and an inside reactor diameter of 0.11 m. The data points shown in Figures 4 to 6 are the actual experimental results at the reactor's exit.

Figure 4 shows that most of the gasification takes place within the first 0.1 m. The computer, also tabulating average particle residence times for the overall coal particle size distribution (which for these tests was standard industrial grind), shows that this length corresponds to an average particle residence time of about 30 ms (shown on the scale at top of the graph). Figure 4 clearly demonstrates the extremely small time scales involved in

hydrogasification with entrained flow-type reactors. Such small time scales dictate the need to have accurate hydrodynamic descriptions of the flow field for suitable reactor modeling.

As discussed earlier, the plug flow hydrodynamic description is quite suitable for reactors using impinging jet-type injectors where good penetration of the reactant jet streams is assured at the point of collision, thereby rapidly producing a uniform one-dimensional flow field with no recirculation. However, for entrained flow reactors using conventional-type injector burner assemblies, hydrodynamical descriptions for reactant mixing should be included.

Figure 5 shows the increase in reactor gas temperature over the reactor's length due to the exothermic nature of the chemical process. Finally, Figure 6 shows the change in gas composition over the reactor's length. Note in the case of Figure 6 that the experimental gas sample was taken on a dry basis, therefore the data points shown at the reactor's exit were determined by correcting the sample for the amount of steam present in the gas, calculated from the computer program.

A result, not shown in Figures 4 to 6 but extremely important, is the fact that the model always estimated the hydrogen partial pressure at the coal particle's surface to be within 90% of the freestream value. This was true for all particles over the entire coal-size distribution and at all stages of devolatilization and gasification. This result would tend to be at variance with those analyses which treat hydrogasification as a two-step process: one of rapid devolatilization followed separately by heterogeneous gasification at the conclusion of pyrolysis. With hydrogen always at the particle's surface, heterogeneous hydrogenation can definitely occur during devolatilization.

The computer calculations also predicted coal particle temperatures exceeding the freestream gas temperature by as much as 300°K during the early rapid stages of hydrogenation. This result may be somewhat high, since the particle's heat of reaction rate, $\dot{Q}_{reac}$, was only given by the exothermic reaction between hydrogen and carbon, while the slight endothermic nature of volatile production was neglected. Also, the rate of heat radiated from the particle's surface, $\dot{Q}_{rad}$, was assumed to be negligible, an assumption which would predict, for this study, slightly higher particle temperatures. However, this significant increase in particle temperature does show that caution should be exercised for analyses which assume the coal particle temperature to be the same as the freestream gas temperature, since this temperature difference can have a measurable effect on the rates of devolatilization and gasification predicted.

The computer model also allowed for the determination of each particle's Biot modulus, a calculation required for the assessment of the uniform particle temperature assumption used in the particle boundary layer analysis. When a particle is undergoing pyrolysis, a modification must be made to the convective heat transfer coefficient used in the calculation of the Biot modulus, since the flow rate of mass away from the particle's surface will block the convective flow of heat from the freestream to the particle. By performing a boundary layer analysis similar to that used earlier in the discussion, it can be shown that the particle's convective heat transfer coefficient, h_{HT}, is given by:

$$h_{HT} = \frac{\dot{m}_p\, c_p}{4\pi r_s^2 \left[\exp\left(\frac{\dot{m}_p\, c_p}{2\, Nu\, \pi\, r_s\, \lambda}\right) - 1\right]} \tag{42}$$

where it has been assumed that the dominant mode of heat transfer inside the particle is by conduction. When $\dot{m}_p$ is zero, it can be seen that Eq. 42 reduces to simply the Nusselt number definition for spheres. For the hydrogasification experimental conditions of this study, it was seen that the Biot modulus ranged from less than 10^{-4} during the initial rapid stages of pyrolysis to 1.0 at zero $\dot{m}_p$ conditions. The Biot modulus was well below 0.1 during most periods where the particle and freestream temperatures were not equal, thus showing the validity of this assumption. For freestream environments other than hydrogen, the Biot modulus would be reduced even further due to the significant decrease in freestream gas thermal conductivity.

Although the computer model correlated the experimental data for the bituminous coals quite well, it could not be adequately verified against results obtained with subbituminous coals. This fact is not surprising considering the behavioral differences of bituminous coals during devolatilization when compared to lignites and subbituminous coals. That is, the plastic behavior associated with many bituminous coals and their associated secondary reaction effects (Anthony and Howard, 1976). In their initial study on coal devolatilization, Anthony et al. (1975) found that pyrolysis yields from lignites were not affected by total system pressure from 10^{-4} to 10 MPa and were able to model their data from a simple kinetic pyrolysis standpoint. Further testing by Suuberg et al. (1978) on lignites has continued to show little if any effect of system pressure on overall lignite conversion.

However, Anthony et al. did find a significant change on bituminous coal conversion with total system pressure, and in a subsequent paper (Anthony et al., 1976) which included hydrogasification, they were able to model their data only after the inclusion of secondary reaction effects. Since the model used in the Rockwell study was developed from the bituminous model of Anthony et al. (1976) and includes these secondary reaction effects, the inability to predict entrained flow subbituminous reactor data is not unexpected, considering subbituminous coals behave more like lignites than bituminous. It is anticipated that the subbituminous reactor data could have been modeled by simply changing the coal chemistry model constants shown in Table 1.

ACKNOWLEDGMENTS

The author would like to express his sincere appreciation to the U.S. Dept. of Energy for the funds allocated in the development of this model under Contract EX-77-C-01-2518; to M.D. Schuman, L. P. Combs, and C. L. Oberg of Rockwell International for their help in the particle boundary layer, bulk flow, and particle chemistry equations, respectively; and to the late J. L. Johnson of the Institute of Gas Technology, and J. B. Howard, H. P. Meissner, and their staff of the Massachusetts Institute of Technology for their time in reviewing much of the current coal chemistry research being conducted at those institutions. Finally, a warm appreciation needs to be extended to J. A. Gray of the Gulf Research and Development Corp. for his help and encouragement during all phases of this model development.

NOTATION

A, A_g = total reactor cross-sectional area and effective gas flow cross-sectional area respectively, m^2
C_D = drag coefficient for spheres
c_p, c_{pc} = specific heat of gaseous species and freestream condensed species respectively, J/kg · K
c_{pp} = specific heat of the particle, J/kg · K
c_1 = k_1/k_c, a constant, Pa^{-1}
c_2 = k_2/k_c, a constant, Pa^{-2}
D = diffusion coefficient, m^2/s
E = activation energy for coal particle pyrolytic reactions, J/mol
E_o = mean activation energy of the activation energy distribution for coal particle pyrolysis, J/mol
E_1 = maximum activation energy of pyrolytic reactions forming nonreactive volatiles or minimum activation energy of pyrolytic reactions forming reactive volatiles, J/mol
h, h_c = enthalpy of gaseous species and freestream condensed species respectively, J/kg
h_p = enthalpy of the coal particle, J/kg
h^o, h_c^o = enthalpy of formation at reference temperature T^o of gaseous species and freestream condensed species respectively, J/kg
h_{afc}^o = enthalpy of formation of the ash-free coal at reference

temperature T^o, J/kg

h_{HT} = particle convective heat transfer coefficient, J/s · m² · K

k = specific reaction rate constant of homogeneous free-stream reactions

k_c = pressure independent reactive volatile mass transfer coefficient, Pa · m³/s

k_o = frequency or pre-exponential factor for coal particle pyrolysis, s^{-1}

k_1 = overall rate coefficient for the reactive volatile deposition reaction, m³/s

k_2 = overall rate coefficient for the hydrogenation reaction of reactive volatiles, m³/Pa · s

k_3 = overall reaction rate constant for the hydrogen-coal heterogeneous reaction, Pa^{-1}

M, M_c = molecular weight of gaseous species and freestream condensed species respectively, g/mol

$\dot{m}$ = mass flow rate of gaseous species through the particle boundary layer, kg/s

$\dot{m}_p$ = particle mass consumption rate, kg/s

$\dot{N}$ = number flow rate of the particles, particle/s

Nu = Nusselt number for heat and mass transfer through the particle's boundary layer

$\dot{n}$, $\dot{n}_c$ = mass freestream flow rate of gaseous and condensed species respectively, kg/s

P = pressure, Pa

$\dot{Q}_{out}$ = rate of heat conducted through the reactor walls, J/s

$\dot{Q}_{rad}$, $\dot{Q}_{reac}$ = rate of heat radiated away from the particle's surface, and absorbed by internal particle reactions respectively, J/s

R = gas constant, J/kg · K

R_u = universal gas constant, 8.317 J/mol · K

Re = Reynolds number for spheres

r, r_s = spatial radial coordinate and particle radius respectively, m

T, T_p, T^o = gas temperature, particle temperature, and species reference temperature respectively, K

t = time, s

u_f, u_p = axial freestream velocity and axial particle velocity respectively, m/s

V = mass of volatiles formed by particle pyrolysis, kg

V^{**} = fraction of original coal mass which can form volatiles

v = mass average velocity of gaseous species in the particle boundary layer relative to the particle, m/s

W^o_{coal} = original or initial as-received mass of the coal particle, kg

Y = gaseous species mass fraction

Z, Z_c = chemical symbol of gaseous species and freestream condensed species respectively

z = spatial axial coordinate, m

ΔH_{coal} = higher heat of combustion per unit mass of as-received coal at reference temperature T^o, J/kg

Δz = distance between axial iteration steps, m

Greek Letters

η = fraction of original coal constituents converted in the coal

η^o = initial mass fraction of coal constituents in the as-received coal

λ = gas thermal conductivity, J/s · m · K

μ = gas dynamic viscosity, kg/m · s

ν', ν'', ν''_c = stoichiometric coefficient for homogeneous free-stream reactions of gaseous reactant species, gaseous product species, and condensed product species respectively

ρ, ρ_c = density of gaseous species and freestream condensed species respectively, kg/m³

ρ_p = apparent density of the coal particle, kg/m³

σ = standard deviation of the activation energy distribution for coal particle pyrolysis, J/mol

$\dot{\omega}$, $\dot{\omega}_c$ = homogeneous species production rate of gaseous species and freestream condensed species respectively, kg/s · m³

Subscripts

ash = ash

CO_2 = carbon dioxide

car = atomic carbon

f = freestream conditions

H_2 = molecular hydrogen

H_2O = water

hv = hydrogenated volatiles

hyd = atomic hydrogen

i = species

j = particle group

k = reaction step

nit = atomic nitrogen

nrv = nonreactive volatiles

ox = atomic oxygen

rv = reactive volatiles

s = particle surface conditions

SO_2 = sulfur dioxide

sul = atomic sulfur

LITERATURE CITED

Abraham, F. F., "Functional Dependence of Drag Coefficient of a Sphere on Reynolds Number," *The Physics of Fluids*, **13**, 2194 (1970).

Anthony, D. B., and J. B. Howard, "Coal Devolatilization and Hydrogasification," *AIChE J.*, **22**, 625 (1976).

Anthony, D. B., J. B. Howard, H. C. Hottel, and H. P. Meissner, "Rapid Devolatilization of Pulverized Coal," *15th Symp. (International) on Combustion*, The Combustion Institute, Pittsburgh, PA, 1303 (1975).

Anthony, D. B., J. B. Howard, H. C. Hottel, and H. P. Meissner, "Rapid Devolatilization and Hydrogasification of Bituminous Coal," *Fuel*, **55**, 121 (1976).

Axworthy, A. E., G. R. Schneider, M. D. Schuman, and V. H. Dayan, *Chemistry of Fuel Nitrogen Conversion to Nitrogen Oxides in Combustion*, EPA-600/2-76-039, Nat. Tech. Info. Service, Springfield, VA (1976).

Blake, T. R., W. D. Henline, and G. P. Schneyer, "Numerical Simulation of Coal Gasification Processes," *AIChE 87th Nat. Meeting*, Boston, MA (1979).

Caram, H. S., and N. R. Amundson, "Diffusion and Reaction in a Stagnant Boundary Layer About a Carbon Particle," *Ind. Eng. Chem. Fundam.*, **16**, 171 (1977).

Combs, L. P., *Liquid Rocket Performance Computer Model with Distributed Energy Release, Final Report*, NASA CR-114462, Nat. Aeronautics and Space Adm., Washington, DC (1972).

El Wakil, M. M., *Experimental and Calculated Temperature and Mass Histories of Vaporizing Fuel Droplets*, NACA Tech. Note No. 3480, Nat. Advisory Comm. for Aeronautics, Washington, DC (1956).

Field, M. A., D. W. Gill, B. B. Morgan, and P. G. W. Hawksley, *Combustion of Pulverized Coal*, BCURA, Leatherhead, England (1967).

Friedman, J., *Development of a Single-Stage, Entrained-Flow, Short-Residence-time Hydrogasifier*, Final Report, FE-2518-24, Nat. Tech. Info. Service, Springfield, VA (1979).

Gordon, S., and B. J. McBride, *Computer Program for Calculation of Complex Chemical Equilibrium Compositions, Rocket Performance, Incident and Reflected Shocks, and Chapman-Jouquet Detonations*, NASA SP-273, Nat. Aeronautics and Space Adm., Washington, DC (1971).

Gray, J. A., P. J. Donatelli, and P. M. Yavorsky, "Hydrogasification Kinetics of Bituminous Coal and Coal Char," *Amer. Chem. Soc.*, Div. of Fuel Chem. Preprints, **20**, No. 4, 103 (1975).

Hirschfelder, J. O., C. F. Curtiss, and R. B. Bird, *Molecular Theory of Gases and Liquids*, John Wiley and Sons, New York (1954).

Huff, V. N., S. Gordon, and V. E. Morrell, *General Method and Thermodynamic Tables for Computation of Equilibrium Composition and Temperature of Chemical Reactions*," NACA Report 1037, Nat. Advisory Comm. for Aeronautics, Washington, DC (1951).

Johnson, J. L., "Kinetics of Coal Gasification in Hydrogen During Initial Reaction Stages," *Amer. Chem. Soc.*, Div. of Fuel Chem. Preprints, **22**, No. 1, 17 (1977).

Oberg, C. L., A. Y. Falk, G. A. Hood, and J. A. Gray, "Coal Liquefaction Under High-Mass Flux and Short-Residence-Time Conditions," *Amer. Chem. Soc.*, Div. of Fuel Chem. Preprints, **22**, No. 2, 185 (1977).

Schuman, M. D., and D. G. Beshore, *Standardized Distributed Energy Release (SDER) Computer Program*, Final Report, I, AFRPL-TR-78-7, Air Force Rocket Propulsion Laboratory, Edwards AFB, CA (1978).
Smith, I. W., "Kinetics of Combustion of Size-Graded Pulverized Fuels in the Temperature Range 1200-2270°K," *Combustion and Flame*, **17**, 303 (1971).
Smoot, L. D., F. D. Skinner, and R. W. Hanks, "Mixing and Reaction of Pulverized Coal in an Entrained Gasifier," *Amer. Chem. Soc.*, Div. of Fuel Chem. Preprints, **22**, No. 1, 77 (1977).
Stull, D. R., and H. Prophet, *JANAF Thermochemical Tables, 2nd ed.*, National Standard Reference Data System, U.S. Government Printing Office, Washington, DC (1971).
Suuberg, E. M., W. A. Peters, and J. B. Howard, "Product Composition and Kinetics of Lignite Pyrolysis," *Ind. Eng. Chem. Process Des. Dev.*, **17**, 37 (1978).
Svehla, R. A., *Estimated Viscosities and Thermal Conductivities of Gases at High Temperatures*, NASA TR R-132, Nat. Aeronautics and Space Adm., Washington, DC (1962).
Ubhayakar, S. K., D. B. Stickler, and R. E. Gannon, "Modelling of Entrained-Bed Pulverized Coal Gasifiers," *Fuel*, **56**, 281 (1977).
Wen, C. Y., and T. Z. Chaung, "Entrainment Coal Gasification Modeling," *Ind. Eng. Chem. Process Des. Dev.*, **18**, 684 (1979).
Wender, I., "Catalytic Synthesis of Chemicals From Coal," *Amer. Chem. Soc.*, Div. of Fuel Chem. Preprints, **20**, No. 4, 16 (1975).
Williams, F. A., *Combustion Theory*, Addison-Wesley, Reading, MA (1965).

Manuscript received November 20, 1979; revision received April 21, and accepted May 7, 1980.

Studies in the Synthesis of Control Structures for Chemical Processes:

Part IV. Design of Steady-State Optimizing Control Structures for Chemical Process Units

YAMAN ARKUN
and
GEORGE STEPHANOPOULOS
Dept. of Chemical Engineering and Materials Science
University of Minnesota
Minneapolis, MN 55455

The design of the steady-state optimizing control for a single unit is formulated within the framework of the nonlinear mathematical programming theory. Alternative implementational strategies are developed and a multilevel screening procedure is proposed to arrive at the best optimizing control configuration. Numerical examples on a fluid catalytic cracking unit and a distillation column demonstrate the systematic design and the synthesis of the most promising optimizing control structures for these systems.

SCOPE

One of the most challenging tasks for a chemical engineer is to design a chemical process that would operate safely in the most profitable fashion to achieve certain design objectives. Subject to varying market conditions, changing raw materials, different product specifications, and other external disturbances, the chemical plant should operate smoothly over a broad range of operating regimes to stay feasible and profitable. The existence of such a dynamic environment around an operating chemical plant necessitates the existence of well designed control structures to maintain or improve the plant operation on-line, in terms of economics, regulation, reliability, and safety aspects.

Control objectives for a chemical process originate from certain regulation tasks (i.e., product quality control, material balance control, safety, environmental regulations, etc.) and economic objectives (i.e., optimizing the economic performance). Such a classification of control objectives automatically formulates the different design activities for the regulatory and optimizing control structures. Whereas regulatory objectives require certain variables to be kept at specified set-points or within permissible bounds, economic objectives will call for optimizing control actions. In the presence of different types of disturbances, optimal set-point values for the controllers have to be determined, and the necessary set-point changes have to be implemented on-line.

In the previous process control structure synthesis methods (Buckley, 1964; Govind and Powers, 1976; Douglas, 1977; Umeda et al. 1978), the distinction between the different classes of control objectives and its impact on the design of the plant control structure have not been addressed. Articles representing the industrial views have recently indicated that, the steady-state optimizing control constitutes the most fruitful

Y. Arkun is presently with the Dept. of Chemical and Environmental Engineering, Rensselaer Polytechnic Institute, Troy, N.Y., 12181.

0001-1541-80-4211-0975-$01.65.